ORIGINAL ARTICLE

WILEY

Preclinical feasibility of robot-assisted sentinel lymph node biopsy using multi-modality magnetic and fluorescence guidance in the head and neck

Giri Krishnan MD[1]　|　Aidan Cousins PhD[2]　|　Nguyen Pham PhD[3]　|
Valentina Milanova PhD[2]　|　Melanie Nelson PhD[4]　|　Shridhar Krishnan MD[5]　|
Nynke S. van den Berg PhD[6]　|　Anil Shetty MD[4]　|　Eben L. Rosenthal MD[6]　|
Peter-John Wormald MD[1]　|　Benjamin Thierry PhD[2]　|　Andrew Foreman MD[1]　|
Suren Krishnan MD[1]

[1]Department of Otolaryngology, Head and Neck Surgery, The University of Adelaide, Adelaide, South Australia, Australia

[2]Future Industries Institute, University of South Australia, Mawson Lakes Campus, Adelaide, South Australia, Australia

[3]Key Centre for Polymers and Colloids, School of Chemistry and University of Sydney Nano Institute, The University of Sydney, Sydney, New South Wales, Australia

[4]Ferronova Pty Ltd, Adelaide, South Australia, Australia

[5]Department of Oral and Maxillofacial Surgery, The University of Adelaide, Adelaide, South Australia, Australia

[6]Department of Otolaryngology—Division of Head and Neck Surgery, Stanford University School of Medicine, Stanford, California, USA

Correspondence
Giri Krishnan, Department of Otolaryngology-Head and Neck Surgery, The University of Adelaide, 28 Woodville Road, Woodville South, SA 5011, Australia.
Email: giri.krishnan@adelaide.edu.au

Abstract

Background: Sentinel lymph node biopsy (SLNB) is a staging procedure dependent on accurate mapping of draining lymphatics via tracers. Robot-assisted SLNB enables access to multiple neck levels with a single incision and intraoperative fluorescence guidance to the SLN.

Methods: Lymphatic mapping in swine was done using a magnetic tracer and fluorescent dye, injected into the tongue. MRI preoperatively mapped lymphatic spread of the magnetic tracer. Dissection was performed using a da Vinci Xi robot guided by fluorescence-imaging of the dye.

Results: Robot-assisted SLNB was successfully performed in all animals ($n = 5$). A novel MRI protocol differentiated SLNs ($n = 6$) from lower echelon nodes ($n = 11$) based on flow progression. Fluorescence imaging provided valuable intraoperative guidance and correlated with magnetic-positive nodes.

Conclusions: This study demonstrates preclinical feasibility of a robot-assisted approach to SLNB using magnetic and fluorescent tracers in the head and neck, enabling both preoperative mapping and intraoperative guidance.

KEYWORDS
indocyanine green, magnetic nanoparticles, robotic surgery, sentinel lymph node biopsy, translational science

Giri Krishnan and Aidan Cousins contributed equally to the study, and are considered joint first authors.

1 | INTRODUCTION

For clinically and radiologically node-negative (cN0) patients with oral and oropharyngeal squamous cell carcinoma (OSCC and OPSCC), accurate detection of positive lymph nodes (LNs) in the neck is critical as there is a 25% chance of micrometastases with an associated 50% decrease in survival.[1,2] The sensitivity of available imaging modalities to detect cervical metastases is only 50%–70%[3]; therefore, elective neck dissection (END) is performed for both staging and treatment. Sentinel lymph node biopsy (SLNB) avoids overtreatment of 75% of cN0 patients by providing equivalent diagnostic yield to END with less morbidity,[4,5]

While SLNB is not broadly considered standard of care for head and neck cancers, the conventional method in which this procedure is performed typically relies on preoperative mapping of radionuclear tracers using scintillation detectors (e.g., lymphoscintigraphy following peritumoral injection of ^{99m}Tc-nanocolloid), and intraoperative guidance to draining LNs via use of handheld gamma probes.[6] A second mode of intraoperative guidance is often also employed using low-molecular weight dyes; for example, visual mapping following blue dye injection, fluorescence imaging using indocyanine green (ICG), or dual-modality ICG-^{99m}Tc-nanocolloids.[6–9]

Despite its potential benefits, SLNB has been poorly adopted in the head and neck, as complexities of lymphatics in this region can make this a technically challenging procedure.[6] For example, guidance with conventional radionuclear tracers and nuclear imaging modalities has anatomic and spatial resolution limitations which can be unsatisfactory, especially for floor of the mouth tumors where level I LNs often lie in close proximity, and where elucidation of LN relationships to neurovascular structures is important.[10,11] While the addition of fluorescence-imaging aims to improve intraoperative detection,[9] radionuclear tracers impose logistical considerations that can significantly impede workflow, such as the need for access to a radiopharmacy in order to produce the tracers; requirements for licensing and training in order to handle, administer, and dispose of the tracers; and the need to plan any preoperative imaging or intraoperative detection around the radioactive half-life of the tracer.

Retention of lymphotropic tracers (such as radiocolloids, magnetic tracers, and dyes) within nodes is typically governed by passive processes—mainly the diffusion of molecules or particles based on size (small particles/molecules transport more quickly than larger ones, and tend to flow-through to lower echelons), and phagocytosis of macrophages within the LN.[12–14] However, the addition of mannose labeling to tracers been has shown to create an additional, active retention process given the abundance of mannose-receptive macrophages within LNs. This concept was translated clinically with the United States Food and Drug Administration (FDA) approval of Lymphoseek (Cardinal Health, Dublin, OH)—a radiolabeled molecule (^{99m}Tc-tilmanocept) which includes a targeting mannose group to reduce flow-through and improve retention in the SLNs.[15]

We recently investigated how the challenges facing SLNB adoption in the head and neck could be addressed by replacing radionuclear tracers with a SLN-specific magnetic nanoparticle (FerroTrace; Ferronova Pty Ltd, Adelaide, SA, Australia).[16] A combination of moderate nanoparticle size (circa 70 nm hydrodynamic diameter) and mannose coating similarly demonstrated reduced flow-through and high retention in the SLNs.[16] With this approach, preoperative lymphoscintigraphy is replaced with magnetic resonance imaging (MRI), and intraoperative detection of SLNs is performed using a combination of visual detection (brown/black discoloration of the nodes resulting from the tracer) and a handheld magnetic-sensing (magnetometer) probe.[16]

As a further step away from the traditional SLNB paradigm, we seek to investigate the feasibility of a robot-assisted approach, where robotic access to multiple nodal levels could be achieved via a modified face-lift approach (MFLA), resulting in an aesthetically pleasing outcome with a single, scar sparing incision hidden in the hairline. Given the high concentration of LNs in the neck, precise intraoperative visualization of the SLN is critical to achieve the required accuracy and to reduce extensive tissue dissection.[17] ICG has previously demonstrated the viable application for robot-assisted neck dissection (RAND) in OSCC patients, guiding dissection to fluorescent SLNs in vivo[18] as well as ex vivo identification of SLNs during pathological sampling.[19] In addition, ICG dye in a dual-modality pairing with radionuclear tracers improves the average detection time of SLNs in non-robotic OSCC,[7] and is particularly beneficial for fluorescing level I SLNs obscured by shine-through radiation in a solely radionuclear approach.[9]

In this study, we investigate progressing the dual-modality approach to RAND by replacing conventional radionuclear tracers with a pairing of a SLN-specific magnetic tracer and ICG dye in a preclinical large animal model.

2 | MATERIALS AND METHODS

2.1 | Animals, anesthesia and monitoring

All animal experiments were performed according to a protocol approved by the Animal Ethics Committee of

the South Australian Health and Medical Research Institute (SAHMRI), ensuring that adequate measures were taken to minimize animal pain or discomfort for the duration of the study. Animal work was performed at SAHMRI facilities in compliance with "The Australian Code of Practice for the Care and Use of Animals for Scientific Purposes, NHMRC" and the ARRIVE guidelines. Five female domesticated pigs (Landrace x Large White) with average weight of 46 ± 2 kg were obtained and maintained according to institutional standards. Animals were anesthetized with 1 mg/kg Xylazil-100 and 10 mg/kg ketamine administered intramuscularly. Endotracheal anesthesia was induced and maintained with 5% and 2% isoflurane, respectively. At the completion of surgery animals were humanely killed with a lethal overdose of intravenous barbiturate.

2.2 | Magnetic and fluorescent tracer

FerroTrace is a suspension of superparamagnetic iron oxide (maghemite) nanoparticles in 0.9% saline designed for SLN mapping, and has recently entered clinical trial in Australia (trial registration number: ACTRN12620000831987). FerroTrace particles are stabilized by a 70:30 mixture of stabilizer and macrophage-targeting (mannose) polymer chains, which results in highly specific binding to the SLN,[16] as well as excellent in vivo stability, biocompatibility, and clearance.[20] These magnetic tracers have very high magnetic susceptibility, which creates strong negative contrast in MRI, and can be detected with handheld magnetometer probes.[21,22] For this study, a novel solid-state magnetometer probe (FerroMag, Ferronova, Adelaide, SA, Australia; Figure 1) was used to confirm the presence of FerroTrace in LNs. Due to the confined surgical field and presence of interfering ferrous metals during robotic surgery, the probe

could not be used intraoperatively; hence, was used for ex vivo measurements only.

For each animal, peritumoral tracer delivery was simulated with submucosal injections of FerroTrace, delivered into the left ventrolateral surface of the tongue using a 29G insulin syringe, bevel up, at an angle of approximately 20° and depth of 5 mm. Injections were divided up into quadrants spaced approximately 10 mm from each other, and centered around a point 50 mm from the tip of the tongue. In addition, each pig received a dose of ICG dye (Cardiogreen, Sigma Aldrich, St Louis, MO) in the same location as FerroTrace injections prior to neck incision (Figure 2). Four of the animals received separate magnetic and ICG injections, consisting of either 0.4 ml (50 mg [Fe]/ml, n = 3) or 0.8 ml (25 mg[Fe]/ml, n = 1) FerroTrace, followed by 0.4 ml (2.5 mg/ml, n = 4) ICG in sterile water for injection. The FerroTrace dose (20 mg[Fe]) was informed by the outcomes of previous preclinical experiments.[16] One animal (animal 4) received a premixed dose of 0.44 ml FerroTrace and ICG (0.34 ml 50 mg[Fe]/ml FerroTrace; 0.1 ml 8 mg/ml ICG), in order to investigate the impact of premixing the two compounds to improve workflow and ensure accurate codelivery of the two agents. In all instances, the FerroTrace dose was delivered while the animal was anesthetized and already in position on the MRI table, approximately 2 h prior to surgery.

2.3 | Preoperative sentinel lymph node mapping

Imaging was performed with a Magnetom Skyra 3.0T MRI (Siemens Healthineers, Erlangen, Germany) using a combination of built-in spine coils and flexible 18-channel body array coils. Two sequences were used: a "pseudo-dynamic" low-TE 2D gradient echo "FLASH" protocol (TE = 2.77; TR = 540; FA = 20°; 3 mm slices)
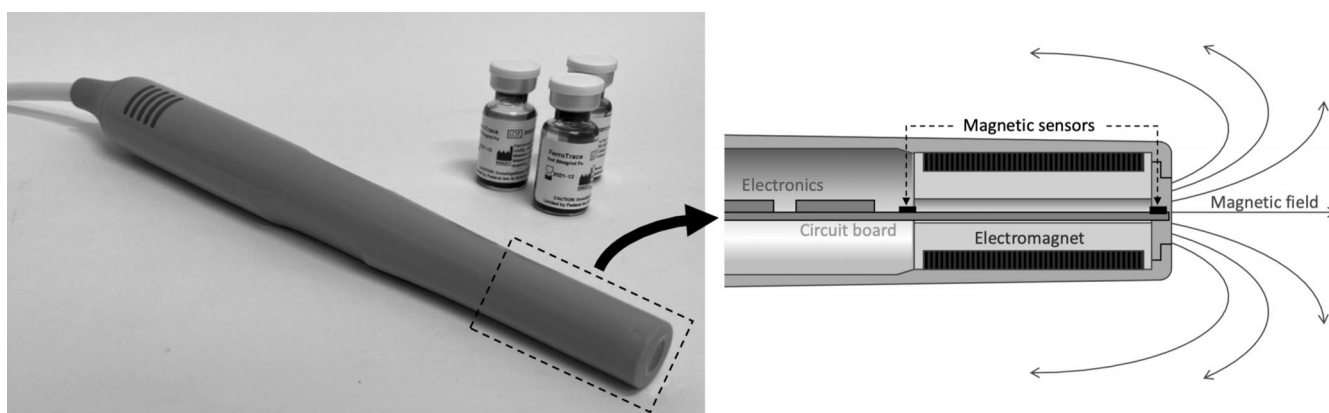

FIGURE 1 (Left) FerroMag solid-state magnetometer probe alongside sealed vials of FerroTrace. (Right) Cross-section view of the magnetometer probe, showing principal components

for fast (100-s) acquisition of scans immediately postinjection, and a "high contrast" modified 2D T2 "FLASH" protocol (TE = 6 ms; TR = 1100 ms; flip angle = 20°; 5 mm slices) for improved anatomical detail and sensitivity to FerroTrace. Animals were scanned prior to injection to achieve a baseline image. Immediately after injection of FerroTrace (1–2 min), a sequence of pseudo-dynamic scans was acquired to map the lymphatic uptake of FerroTrace over the course of 10–15 min. Both imaging protocols were repeated at 15-min and 1-h postinjection. The SLNs were defined as the LNs that drained directly from the injection site, and hence were identified as the first LNs to produce a negative contrast on MRI as a result of FerroTrace uptake.

2.4 | Robot-assisted sentinel lymph node biopsy procedure

Pigs were positioned in a lateral decubitus position on the operating table to best replicate the standard extended and laterally rotated neck position used for human neck dissection. The skin incision began behind the pinna and was carried forward and then posteroinferiorly behind the ramus of the mandible (Figure 2) to replicate a hairline MFLA used for RAND in humans.[23] Subplatysmal flaps were raised with monopolar diathermy to expose the three-cornered parotid gland to the masseter muscle anteriorly, the angle of mandible and sternohyoid muscle inferiorly and the sternocleidomastoid and trapezius muscles posteriorly (Figure 2).

A da Vinci Xi surgical system was docked on the contralateral side of the bed to the side of neck dissection (Figure 2). Vision was provided by a 30° endoscopic camera equipped with "Firefly" technology for ICG fluorescence imaging. A 5 mm Maryland forceps was introduced on the left side and harmonic curved shears on the right side. Dorsal flaps were retracted with a silk suture and ventral flaps were retracted by an assistant with 5-inch langenbeck retractors.

SLNB was performed by targeted dissection of individual LNs in order of afferent tracer drainage from the injection site as identified by preoperative MRI. The pig typically has 3 LN groups that drain from the oral tongue:
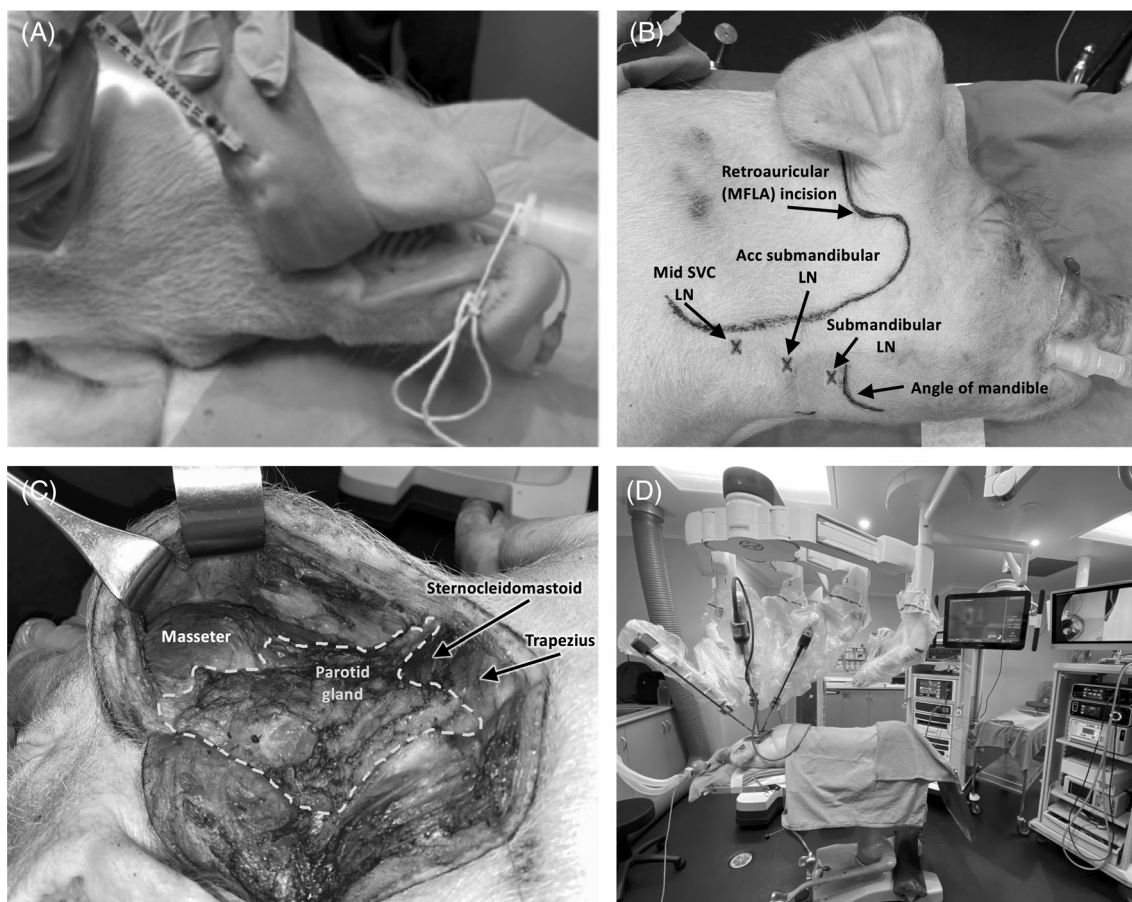

FIGURE 2 Representative workflow of robot-assisted dissection. (A) Injection of tracer in a quadrant in the left anterior ventrolateral tongue. (B) Neck incision marking for retroauricular approach designed to simulate a modified-face lift incision. (C) Demonstration of dissection tunnel with key anatomic landmarks exposed following skin incision and raising of subplatysmal flaps. (D) The da Vinci Xi robot is docked, with endoscope and instruments placed into the dissection tunnel. LN, Lymph node; MFLA, modified face-lift approach

The submandibular LN; the accessory mandibular LN; and the superficial ventral cervical (SVC) chain of LNs, which include the cranial, middle and caudal LNs.[24]

Visual confirmation of positive LNs was informed by both Firefly fluorescence imaging as ICG flowed through lymphatics, and by dark brown/black discoloration of LNs from FerroTrace. All LNs identified on preoperative MRI were dissected with the robot and delivered from the dissection tunnel with forceps. The drainage order of lower echelon LNs was determined based on tracer uptake as seen on pseudo-dynamic MRI, the LN group, or the source of afferent drainage. For example, the different chains of SVC LNs are anatomically quite close to each other, however ICG mapping may show the middle SVC LNs draining into the cranial SVC LNs; hence in this instance the former would be considered second echelon, and the latter considered third echelon.

2.5 | Open exploration and ex vivo lymph node analysis

After completion of the robot-assisted SLNB, an open neck exploration was performed on both sides of the neck to inspect the surgical site for additional fluorescent LNs using a Stryker 1688 "AIM" fluorescent camera system (Stryker, Kalamazoo, MI). Any additional lower echelon, ICG-positive LNs were removed and used to determine the relative specificity of the FerroTrace magnetic tracer. All individually excised LNs underwent "closed-field" fluorescent imaging using the Stryker camera in a pitch-dark room at a fixed distance and camera setting for all LNs. Mean fluorescence intensity (MFI) was calculated using MATLAB (MathWorks, Natick, MA) from regions of interest drawn around captured LN images. These values were normalized to the total MFI measured in a draining basin (each side of the neck was treated independently). The ex vivo magnetometer signal was measured by holding the probe vertically-upwards and individually placing each LN on the tip of the probe. The sample was moved around until the maximum signal was measured, and this process was repeated three times for each sample to record an average value. As with fluorescence signals, the magnetometer values were normalized to the total signal in the draining basin.

3 | RESULTS

3.1 | Preoperative magnetic resonance imaging mapping

Uptake of FerroTrace into the lymphatics was seen immediately following injection, via the use of low-TE pseudo-dynamic sequences. Over the course of the pseudo-dynamic scans, contrast between draining LNs and surrounding tissue progressively increased (Figure 3). Contrast continued to increase up to the 1-h postinjection timepoint, indicating a prolonged uptake of the magnetic tracer into LNs over this time. This protocol also provided a temporal resolution of 100 s between scans, and as such could be used to identify sentinel, secondary, and tertiary echelon LNs in a manner analogous to lymphoscintigraphy (Figure 3). After 1 h, a mean of 2.8 ± 1.6 LNs per neck were identified with preoperative MRI. Of the MRI-positive LNs, there was an average of 1.0 ± 0.0 SLNs ($n = 6$), 1.3 ± 1.0 s echelon LNs ($n = 8$), and 0.5 ± 0.8 third echelon LNs ($n = 3$) per neck.

3.2 | Robot-assisted approach

Robot-assisted SLNB was successfully performed in all five pigs. Preoperative MRI provided excellent anatomic resolution and the ability to differentiate SLNs from lower echelons. This allowed clear planning of approach to SLN locations in relation to bony, vascular and soft tissue landmarks. From a feasibility standpoint, the simulated MFLA incision and dissection tunnel provided adequate access to all targeted LN groups. All blood vessels encountered were controlled with diathermy or surgical clips and blood loss was minimal. There were no operative complications and all animals survived to completion of procedure.

As has been noted by others,[25] the set-up time for robotic surgery was longer than for open dissection, and first-time users of the robot were presented with a learning curve as they adjusted to the tunneling approach. However, the introduction of ICG dye and use of the Firefly camera significantly aided dissection, providing excellent guidance to draining LNs embedded deep within tissue (Figure 4). Although the magnetometer probe could not be used intraoperatively, magnetic-positive LNs still provided a characteristic dark discoloration, which could be visualized on brightfield imaging (Figure 4).

3.3 | Open exploration and ex vivo measurements

Following RAND SLNB, the procedure was converted to open exploration to locate lower echelon LNs containing ICG, but not identified on MRI. This dissection identified an additional 13 LNs which received ICG; hence, a total of 30 LNs were ICG-positive, with a mean and standard deviation of 4.3 ± 1.6 per neck. Note that in one animal (animal 3), FerroTrace drained contralaterally, while ICG
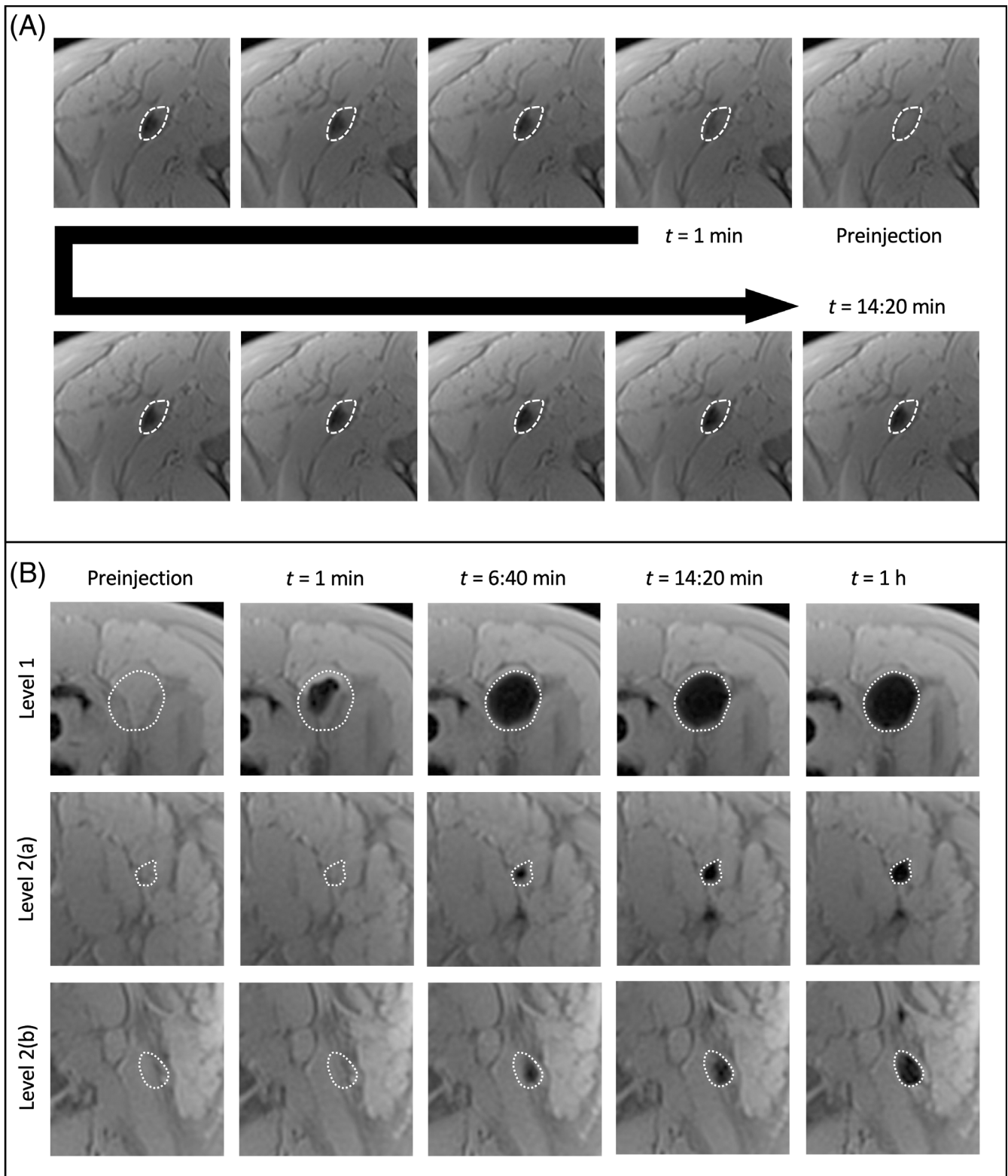
FIGURE 3 Demonstration of the pseudo-dynamic preoperative MRI sequence. (A): Progressive uptake of FerroTrace into the sentinel node after injection, as viewed on pseudo-dynamic scans acquired every 100 s. (B) Using MRI to differentiate levels in the neck and identify the SLN. Over the duration of the pseudo-dynamic sequence (8 scans over 13 min), there is a clear pattern of drainage from the SLN (seen 1-min postinjection) down to lower echelon nodes (both appearing approximately 5 min after the SLN). SLN, sentinel lymph node
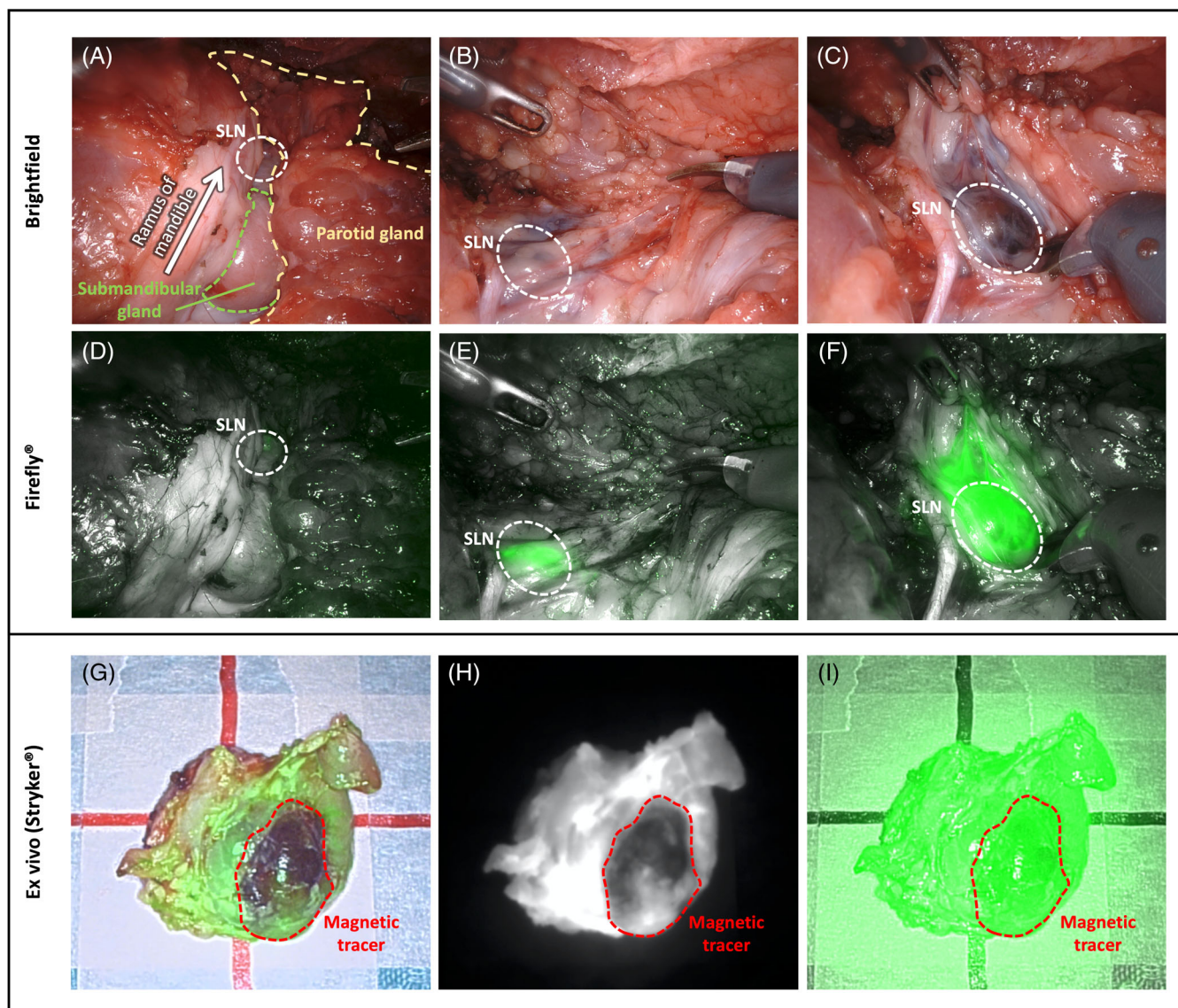
FIGURE 4 (A–F) Endoscopic steps of robot-assisted SLN biopsy viewed in brightfield (A–C) and Firefly (D–F). The submandibular node is accessed by skeletonizing the anterior edge of the parotid gland at the angle of the mandible and retracting it posteriorly and dissecting deep to the submandibular gland. Note, when the node is completely exposed, a dark brown discoloration can be seen (C), resulting from the accumulation of magnetic tracer within the node. (G–I) The impact of a concentrated FerroTrace accumulation (outlined with red dashed line) on ICG fluorescence signal, as measured with the Stryker AIM system: low-sensitivity ICG color overlay (G); low-sensitivity near-infrared "contrast" mode signal (H); high-sensitivity false-color "ENV mode" ICG overlay (I). ICG, indocyanine green; SLN, sentinel lymph node [Color figure can be viewed at wileyonlinelibrary.com]

drained bilaterally. In this instance, variations in lymphatic drainage may have been influenced by the tracer dynamics (if left longer, some FerroTrace may have been detected in the left neck) or as a consequence of delivering the two tracers via separate injections (imperfect codelivery, which could be improved by premixing the tracers).

The relative signal strengths from magnetometer probe and MFI were calculated and each LN graded based on discoloration from FerroTrace (Table 1). Using relative magnetic signal levels, FerroTrace indicated specificity to the SLN, with $75 \pm 22\%$ ($n = 5$) of the magnetometer signal occurring in the SLN, with a stratification of signal strength between sentinel and lower echelon LNs observed.

4 | DISCUSSION

To the best of our knowledge this study presents the first description of a robot-assisted SLNB procedure in the head and neck with multi-modal guidance.[26] Here we

TABLE 1 Details acquired from ex vivo analysis of removed lymph nodes using visual coloration, magnetometer signal, and indocyanine green fluorescence intensity

Pig	MRI positive LNs	Identification modality	Color grading	Draining order	Magnetic signal[a]	MFI signal[a]
1	L submandibular	Magnetic/ICG	Dark	SLN	100%	68%
	L acc submandibular	ICG	–	2nd echelon	–	12%
	L middle SVC	ICG	–	2nd echelon	–	20%
	R submandibular	Magnetic/ICG	Dark	SLN	71%	46%
	R middle SVC (a)	Magnetic/ICG	Mild	2nd echelon	29%	20%
	R middle SVC (b)	Magnetic/ICG	Mild	2nd echelon	BT	17%
	R acc submandibular	ICG	–	2nd echelon	–	6%
	R caudal SVC	ICG	–	3rd echelon	–	4%
	R cranial SVC	ICG	–	3rd echelon	–	7%
2	L submandibular	Magnetic/ICG	Dark	SLN	67%	34%
	L middle SVC (a)	Magnetic/ICG	Dark	2nd echelon	10%	35%
	L middle SVC (b)	Magnetic/ICG	Dark	2nd echelon	12%	17%
	L cranial SVC	Magnetic/ICG	Dark	3rd echelon	11%	13%
3	L submandibular	ICG	–	SLN	–	68%
	L acc submandibular	ICG	–	2nd echelon	–	16%
	L middle SVC	ICG	–	2nd echelon	–	16%
	R acc mandibular	Magnetic/ICG	Mild	SLN	BT	64%
	R submandibular	ICG	–	SLN[b]	–	27%
	R middle SVC	ICG	–	2nd echelon	–	9%
4	L submandibular	Magnetic/ICG	Dark	SLN	92%	53%
	L caudal SVC	Magnetic/ICG	Mild	2nd echelon	8%	24%
	L middle SVC (a)	Magnetic/ICG	Mild	2nd echelon	BT	17%
	L middle SVC (b)	ICG	–	2nd echelon	–	5%
5	R submandibular	Magnetic/ICG	Dark	SLN	43%	41%
	R middle SVC (a)	Magnetic/ICG	Dark	2nd echelon	21%	14%
	R middle SVC (b)	Magnetic/ICG	Dark	2nd echelon	28%	7%
	R cranial SVC (a)	Magnetic/ICG	Dark	3rd echelon	7%	23%
	R cranial SVC (b)	Magnetic/ICG	Dark	3rd echelon	1%	9%
	R middle SVC (c)	ICG	–	2nd echelon	–	1%
	R cranial SVC (c)	ICG	–	3rd echelon	–	5%

Abbreviations: acc, accessory; BT, below threshold false negative reading; L, left; MFI, mean fluorescence intensity; R, right; SVC, superficial ventral cervical.
[a]Measured relative to the total accumulated signal in that basin (left and right neck treated independently).
[b]Suspected coincident drainage, as submandibular node is superior to the accessory node.

demonstrate in a porcine model the technical feasibility of a single retroauricular incision to provide access to all targeted nodal groups, and describe a workflow that involves preoperative MRI, intraoperative fluorescence-imaging guidance (with optional visual identification), and confirmation of the SLN with a magnetometer probe.

Developing on our previous work developing a SLN-specific magnetic tracer,[16] the addition of intraoperative ICG-guidance in this study proved particularly beneficial, providing a clear roadmap of highlighted lymphatic vessels and the progression through first, second, and third echelon draining LNs with excellent anatomic resolution. We found this essential to robot-assisted dissection, which, without the wide field of view afforded by conventional neck dissection, relied heavily on local reference structures (i.e., fluorescent lymphatic vessels) to guide the surgeon. Previous studies using ICG for robot-assisted SLNB successfully demonstrated the utility of this fluorescent dye to sample SLNs either pre- or post-RAND, but did not have the ability to provide preoperative SLN imaging.[18,19] As such, we believe that clinical translation of our proposed approach would both limit the extent of

robotic dissection and the number of LNs sent for detailed histopathological analysis, and conform with the wide belief that the gold-standard for SLNB requires the use of both preoperative and intraoperative SLN detection methods.[9,27-29] Furthermore, while we believe that the workflow described for the magnetic-ICG approach is particularly suited to robot-assisted SLNB, it is also applicable to conventional SLNB in the head and neck, where the use of intraoperative fluorescence-imaging guidance creates an additional modality with which to identify draining lymphatic vessels and to differentiate SLNs from surrounding tissue in vivo.

In order to best understand the potential benefits and limitations of our magnetic-ICG approach, we were particularly interested in studying the quantifiable characteristics of both tracers. For instance, when comparing the number of LNs per neck basin (to account for instances of bilateral drainage), FerroTrace resulted in a mean and standard deviation of 2.8 ± 1.6 magnetic LNs per neck, compared to 4.3 ± 1.6 ICG LNs per neck. This demonstrates a reduced flow-through of FerroTrace compared to the low molecular weight ICG dye, implying greater LN retention and specificity. There appeared to be no significant difference in LN numbers when FerroTrace was premixed with ICG (animal 4; 3 magnetic LNs, 4 ICG LNs).

The result of premixing ICG with the commercially available magnetic tracer "Magtrace" (Endomag, Cambridge, UK) has been briefly described elsewhere.[30] In this instance, premixing created a non-covalent binding of ICG to the carboxydextran coating of Magtrace nanoparticles, resulting in a concurrence between fluorescent and magnetic signals.[30] For our study, premixing Ferro-Trace and ICG dye was performed to more broadly test if this would result in any significant changes to fluorescence, magnetic signals, or tracer dynamics. Given the markedly different coatings of Magtrace and FerroTrace (the latter using polyacrylamide and polyethelyneglycol polymers), a similar binding effect of ICG to FerroTrace cannot be assumed, and additional work would be required to study this. In addition, more accurately determining the relative specificity of FerroTrace compared to ICG dye is a goal for future studies, which would benefit from more extensive dissection of the neck to remove additional lower echelon LNs (e.g., lateral retropharyngeal and medial cervical nodes[24]).

While the magnetometer probe was useful for ex vivo confirmation of magnetic signals, for this study the advantage of solid-state magnetometers (very high spatial resolution, which is less important for ex vivo application) is somewhat outweighed by the corresponding drawbacks (shorter detection range and lower sensitivity compared to coil-based magnetometers). This is

evidenced by the accuracy rate of the magnetometer, detecting 83% (5/6) of SLNs, and 82% (14/17) of all magnetic LNs (Table 1). In our previous preclinical work,[16] we demonstrated that following FerroTrace injection, an average accumulation of $83 \pm 13\%$ of the lymphotropic iron retains in the SLN, which corresponded to $77 \pm 16\%$ of the magnetometer signal. While iron content was not evaluated in this present study, the relative SLN magnetometer signals ($75 \pm 22\%$) were consistent with our previous work. With a more sensitive and longer-ranging magnetometer probe (e.g., coil-based), influences that affect signal strength of the solid-state probe employed here (node size, distribution of tracer within the node, excess adipose tissue[21]) are likely to lessen, and one expects the relative magnetometer signal to more closely approximate that of iron uptake.[31] As such, in settings where pseudo-dynamic MRI is not possible or where the first MRI scan shows multiple draining LNs, we propose that magnetometer signal stratification between node levels could be used to identify the SLN and potentially provide a signal threshold level—such as the "10%" criterion opted to help define magnetic SLNs in breast cancer.[32] In addition, future development of specialized "drop-in" probes could aid intraoperative signal confirmation during robotic or laparoscopic SLNB, as has been demonstrated with gamma-guidance in the abdomen and pelvis[33] and is currently being researched for magnetic-guidance using novel magnetometer probe designs.[34,35]

During surgery, when fluorescent LNs were uncovered, the dark brown/black color of FerroTrace iron oxide nanoparticles fulfilled a role similar to blue dye, whereby SLNs were clearly stained and discernible on bright field imaging (Figure 4). This created an optional modality, whereby the dark stain could heuristically differentiate SLNs from lower echelon nodes with lesser FerroTrace uptake. An interpretation of the ICG data, whereby the relative fluorescence intensity is used to approximate accumulation levels, was initially hypothesized as a means for comparing levels of uptake between the two tracers. However, it was observed during this study that FerroTrace particles in high concentrations attenuated some of the fluorescent signal (Figure 4). The predominant cause of this attenuation is likely to be FerroTrace particles absorbing and scattering both camera excitation (789 nm) and ICG dye emission (819 nm) wavelengths. Fortunately, both Firefly and Stryker AIM cameras have an adjustable sensitivity level, and while the impact of FerroTrace particles is evident on low sensitivity settings, it is significantly reduced by adjusting to a higher sensitivity level (Figure 4). In addition, the ICG dye tended to diffuse throughout the whole LN, whereas FerroTrace tended to be locally accumulated in a high concentration. As such, we did not report any incidences

where the presence of FerroTrace prevented fluorescent identification of a draining LN.

In general, our proposed magnetic-ICG combination delivers significant benefits over dual-modality approaches using radionuclear tracers. For instance, magnetic tracers do not require consideration of the logistics behind manufacturing, transport, decay half-life, or hazards associated with radionuclear tracers, thus provide flexibility and control over administration and timing of injection, imaging, and surgery. Another benefit is that magnetic tracers allow independence in surgical planning because of the clear contrast between endogenous tissue and exogenous magnetic particles on MRI scans, and the excellent anatomic and soft-tissue detail afforded by preoperative MRI compared to radionuclear imaging methods (lymphoscintigraphy and SPECT). In addition, for this study we validated a pseudo-dynamic MRI protocol, which has the ability to identify the SLN based on the progression of lymphatic spread of FerroTrace in a manner analogous to lymphoscintigraphy. Figure 3 demonstrates this utility, where the temporal resolution afforded by the MRI sequence provides clear differentiation between the SLN and lower echelon LNs based on progressive tracer accumulation. While this preclinical study can make use of serial MRI scans to progressively map lymphatic flow through multiple levels, in clinical practice the use of multiple scans may not be necessary. Instead, these sequences may be better utilized to define SLNs from lower echelon LNs by imaging shortly after injection (e.g., 1–3 min postinjection, capturing SLNs only), and then again at a sufficient time interval (e.g., 30 min or more, capturing both SLNs and lower echelon LNs).

Overall, the combined magnetic-ICG approach described in this study presents an improved strategy for SLNB, creating opportunities for both preoperative mapping via MRI, and sensitive intraoperative guidance via fluorescence-imaging. It is hoped that the introduction of a retroauricular robot-assisted approach could improve aesthetic results and circumvent the difficulties with incision placement and nodal access that have been major short-comings of conventional SLNB in the head and neck. However, there remains, significant clinical work in order to validate the potential benefits of magnetic-ICG, robot-assisted SLNB in the head and neck, and a case for using a robot for this procedure needs to be weighed against its substantial added cost. From a resource utilization standpoint, an economically feasible case could be made for patients with cN0 oropharyngeal cancer being treated with TORS, where a combination of preoperative MRI and robotic primary resection followed by a minimally-invasive robot-assisted SLNB approach could optimize robotic theater utilization and reduce surgical time and complications.[36] More practically, future clinical translation of the multi-modal approach to SLNB (robot-assisted or conventional) should aim at refining protocols for the timing and dose of ICG and magnetic tracer injections. In addition, the impact to the normal clinical workflow should be considered, such as the feasibility of timing MRI to minimize latency between injection and the first pseudo-dynamic scan (i.e., consider performing patient injection on the MRI table), and the timing of MRI relative to the surgery (e.g., same-day vs. next-day surgery).

CONFLICT OF INTEREST

All conflicts listed below were at the time of research, and preparation of the original manuscript: Giri Krishnan, Aidan Cousins and Benjamin Thierry have financial interests in Ferronova. Melanie Nelson and Anil Shetty are employees of Ferronova. Aidan Cousins, Valentina Milanova, and Nguyen Pham are consultants for Ferronova, and receive employment through joint collaborations between Ferronova and their institute. Giri Krishnan, Aidan Cousins, Nguyen Pham, Valentina Milanova, Andrew Foreman, Benjamin Thierry, and Nynke van den Berg serve as scientific advisors for Ferronova.

ORCID
Aidan Cousins https://orcid.org/0000-0002-2986-422X

REFERENCES

1. Motiee-Langroudi M, Amali A, Saedi B, et al. Occult level IV metastases in clinically node-negative patients with oral tongue squamous cell carcinoma. *J Laryngol Otol.* 2016;130(5):474-477.

2. Yang S, Wang D, Wang X, Mao C. Positive lymph node ratio is an important prognostic factor of oral squamous cell carcinoma. *Chin J Stomatol.* 2016;51(3):133-136.

3. Alberico RA, Husain SHS, Sirotkin I. Imaging in head and neck oncology. *Surg Oncol Clin.* 2004;13(1):13-35.

4. Colevas AD, Yom SS, Pfister DG, et al. *NCCN Guidelines Insights: Head and Neck Cancers*, Version 1.2018; 2018.

5. Liu M, Wang SJ, Yang X, Peng H. Diagnostic efficacy of sentinel lymph node biopsy in early oral squamous cell carcinoma: a meta-analysis of 66 studies. *PLoS One.* 2017;12(1):e0170322.

6. Pitman KT, Ferlito A, Devaney KO, Shaha AR, Rinaldo A. Sentinel lymph node biopsy in head and neck cancer. *Oral Oncol.* 2003;39(4):343-349.

7. Nakamura T, Kogashiwa Y, Nagafuji H, Yamauchi K, Kohno N. Validity of sentinel lymph node biopsy by ICG fluorescence for early head and neck cancer. *Anticancer Res.* 2015; 35(3):1669-1674.

8. Paredes P, Vidal-Sicart S, Campos F, et al. Role of ICG-^{99m}Tc-nanocolloid for sentinel lymph node detection in cervical cancer: a pilot study. *Eur J Nucl Med Mol Imaging.* 2017;44(11): 1853-1861.

9. van den Berg NS, Brouwer OR, Klop WMC, et al. Concomitant radio- and fluorescence-guided sentinel lymph node biopsy in squamous cell carcinoma of the oral cavity using ICG-(99m)Tc-nanocolloid. *Eur J Nucl Med Mol Imaging.* 2012;39(7):1128-1136.

10. Koch WM, Choti MA, Civelek AC, Eisele DW, Saunders JR. Gamma probe–directed biopsy of the sentinel node in oral squamous cell carcinoma. *Arch Otolaryngol Head Neck Surg.* 1998;124(4):455-459.

11. Payoux P, Dekeister C, Lopez R, Lauwers F, Esquerré JP, Paoli JR. Effectiveness of lymphoscintigraphic sentinel node detection for cervical staging of patients with squamous cell carcinoma of the head and neck. *J Oral Maxillofac Surg.* 2005; 63(8):1091-1095.

12. Bluemel C, Herrmann K, Giammarile F, et al. EANM practice guidelines for lymphoscintigraphy and sentinel lymph node biopsy in melanoma. *Eur J Nucl Med Mol Imaging.* 2015;42(11): 1750-1766.

13. Pouw JJ, Ahmed M, Anninga B, et al. Comparison of three magnetic nanoparticle tracers for sentinel lymph node biopsy in an in vivo porcine model. *Int J Nanomedicine.* 2015;10:1235.

14. Cousins A, Thompson SK, Wedding AB, Thierry B. Clinical relevance of novel imaging technologies for sentinel lymph node identification and staging. *Biotechnol Adv.* 2014;32(2):269-279.

15. Surasi DS, O'Malley J, Bhambhvani P. 99mTc-Tilmanocept: a novel molecular agent for lymphatic mapping and sentinel lymph node localization. *J Nucl Med Tech.* 2015;43(2):87-91.

16. Krishnan G, Cousins A, Pham N, et al. Preclinical evaluation of a mannose-labeled magnetic tracer for enhanced sentinel lymph node retention in the head and neck. *Nanomedicine.* 2022;42:102546.

17. de Bree R, Takes RP, Castelijns JA, et al. Advances in diagnostic modalities to detect occult lymph node metastases in head and neck squamous cell carcinoma. *Head Neck.* 2015;37(12): 1829-1839.

18. Chow VL-Y, Ng JC-W, Chan JY-W, Gao W, Wong T-S. Robot-assisted real-time sentinel lymph node mapping in oral cavity cancer: preliminary experience. *J Robot Surg.* 2020;15(3): 349-353.

19. Kim JH, Byeon HK, Kim DH, Kim S-H, Choi EC, Koh YW. ICG-guided sentinel lymph node sampling during robotic retro-auricular neck dissection in cN0 oral cancer. *Otolaryngol Head Neck Surg.* 2020;162(3):410-413.

20. Pham BT, Colvin EK, Pham NT, et al. Biodistribution and clearance of stable superparamagnetic maghemite iron oxide nanoparticles in mice following intraperitoneal administration. *Int J Mol Sci.* 2018;19(1):205.

21. Cousins A, Balalis GL, Thompson SK, et al. Novel handheld magnetometer probe based on magnetic tunnelling junction sensors for intraoperative sentinel lymph node identification. *Sci Rep.* 2015;5(1):10842.

22. Gloag L, Mehdipour M, Ulanova M, et al. Zero valent iron core-iron oxide shell nanoparticles as small magnetic particle imaging tracers. *Chem Commun (Camb).* 2020;56(24):3504-3507.

23. Park YM, Holsinger FC, Kim WS, et al. Robot-assisted selective neck dissection of levels II to V via a modified facelift or retro-auricular approach. *Otolaryngol Head Neck Surg.* 2013;148(5): 778-785.

24. Saar LI, Getty R. The interrelationship of the lymph vessel connections of the lymph nodes of the head, neck, and shoulder regions of swine. *Am J Vet Res.* 1964;25:618-636.

25. Garg A, Dwivedi RC, Sayed S, et al. Robotic surgery in head and neck cancer: a review. *Oral Oncol.* 2010;46(8):571-576.

26. Accorona R, D'Onghia A, Pignataro L, Capaccio P. Head and neck robotic surgery combined with sentinel lymph node biopsy. Fascinating, but feasible? *Oral Oncol.* 2020;111:104939.

27. Acar C, Kleinjan GH, van den Berg NS, Wit EMK, van Leeuwen FWB, van der Poel HG. Advances in sentinel node dissection in prostate cancer from a technical perspective. *Int J Urol.* 2015;22(10):898-909.

28. Alex JC. The application of sentinel node radiolocalization to solid tumors of the head and neck: a 10-year experience. *Laryngoscope.* 2004;114(1):2-19.

29. Ingo S, Joachim D, Thorsten P, Dirk S, Joachim K. Intraoperative fluorescence imaging for sentinel lymph node detection: prospective clinical trial to compare the usefulness of Indocyanine green vs technetium Tc 99m for identification of sentinel lymph nodes. *Arch Surg (Chicago 1960).* 2015;150(7):617.

30. Azargoshasb S, Molenaar L, Rosiello G, et al. Advancing intraoperative magnetic tracing using 3D freehand magnetic particle imaging. *Int J Comput Assist Radiol Surg.* 2022;17(1): 211-218.

31. Ahmed M, Anninga B, Pouw JJ, et al. Optimising magnetic sentinel lymph node biopsy in an in vivo porcine model. *Nanomed Nanotechnol Biol Med.* 2015;11(4):993-1002.

32. Hersi A-F, Pistiolis L, Dussan Luberth C, et al. Optimizing dose and timing in magnetic tracer techniques for sentinel lymph node detection in early breast cancers: the prospective multicenter SentiDose trial. *Cancers (Basel).* 2021; 13(4):693.

33. van Oosterom MN, Simon H, Mengus L, et al. Revolutionizing (robot-assisted) laparoscopic gamma tracing using a drop-in gamma probe technology. *Am J Nucl Med Mol Imaging.* 2016; 6(1):1-17.

34. Kuwahata A, Tanaka R, Matsuda S, et al. Development of magnetic probe for sentinel lymph node detection in laparoscopic navigation for gastric cancer patients. *Sci Rep.* 2020; 10(1):1798.

35. van de Loosdrecht MM, Waanders S, Krooshoop HJG, ten Haken B. Separation of excitation and detection coils for in vivo detection of superparamagnetic iron oxide nanoparticles. *J Magn Magn Mater.* 2019;475:563-569.

36. Byrd JK, Paquin R. Cost considerations for robotic surgery. *Otolaryngol Clin North Am.* 2020;53(6):1131-1138.